TITLE

Left Hemisphere Dominance for Bilateral Kinematic Encoding in the Human Brain

AUTHORS:

Christina M. Merrick[1*], Tanner C. Dixon[2], Assaf Breska[1], Jack J. Lin[3], Edward F., Chang[4], David King-Stephens[5], Kenneth D. Laxer[5], Peter B. Weber[5], Jose M. Carmena[2,6,7], Robert T. Knight[1,2,4,7], Richard B. Ivry[1,2,7]

AFFILIATIONS:

[1] Department of Psychology, University of California, Berkeley, CA, USA

[2]UC Berkeley – UCSF Graduate Program in Bioengineering

[3]Department of Neurology, University of California at Irvine, Irvine, CA, USA.

[4]Department of Neurological Surgery, University of California San Francisco, San Francisco, CA, USA.

[5]Department of Neurology and Neurosurgery, California Pacific Medical Center, San Francisco, CA, USA.

[6]Department of Electrical Engineering and Computer Sciences, University of California, Berkeley, CA, USA

[7]Helen Wills Neuroscience Institute, University of California, Berkeley, CA, USA

*Correspondence: cmerrick@berkeley.edu

KEYWORDS: lateralization; left hemisphere; motor control; reaching movements; ipsilateral; praxis; electrocorticography

ABSTRACT

Neurophysiological studies in humans and non-human primates have revealed movement representations in both the contralateral and ipsilateral hemisphere. Inspired by clinical observations, we ask if this bilateral representation differs for the left and right hemispheres. Electrocorticography (ECoG) was recorded in human participants during an instructed-delay reaching task, with movements produced with either the contralateral or ipsilateral arm. Using a cross-validated kinematic encoding model, we found stronger bilateral encoding in the left hemisphere, an effect that was present during preparation and was amplified during execution. Consistent with this asymmetry, we also observed better across-arm generalization in the left hemisphere, indicating similar neural representations for right and left arm movements. Notably, these left hemisphere electrodes were largely located over premotor and parietal regions. The more extensive bilateral encoding in the left hemisphere adds a new perspective to the pervasive neuropsychological finding that the left hemisphere plays a dominant role in praxis.

INTRODUCTION

A primary tenet of neurology is the contralateral organization of movement. The vast majority of the fibers from the corticospinal tract cross to the opposite side of the body (Nyberg-Hansen & Rinvik, 1963) and functionally, hemiparesis resulting from cortical stroke is manifest on the contralateral side of the body (Bourbonnais, & Noven, 1989). Although direct control of arm movements is primarily mediated through contralateral projections, unimanual arm movements elicit bilateral activity in the primary motor cortex (M1, Babiloni et al., 1999; Ghacibeh et al., 2007), indicating that neural activity in the ipsilateral hemisphere contains information relevant to ongoing movement. Correspondingly, kinematic and movement parameters of the ipsilateral limb can be decoded from ipsilateral hemisphere intracortical recordings in monkeys (Ganguly et al., 2009; Ames & Churchland, 2019) and from electrocorticography (ECoG) in humans (Bundy, Szrama, Pahwa & Leuthardt, 2018; Ganguly et al., 2009, Wisneski et al., 2008). Ipsilateral signals represent an intriguing source of neural activity, both for understanding how activity across the two hemispheres results in coordinated movement and because this information might be exploited for rehabilitative purposes.

While it is established that information about unimanual movements is contained within the ipsilateral hemisphere, there remains considerable debate about what this signal represents. Previous studies have centered on the question of whether ipsilateral representations overlap or are independent of contralateral representations, leading to mixed results. Consistent with the overlap hypothesis, neural activity for the contralateral and ipsilateral limb movements show several similarities, including shared target tuning preferences and the ability to cross predict kinematic features from a model trained on the opposite arm (Bundy, Szrama, Pahwa & Leuthardt, 2018; Cisek, Crammond & Kalaska, 2003; Steinberg et al., 2002, Willett et al., 2020). Consistent with the independence hypothesis, intracortical recordings in monkeys have revealed that the lower dimensional representations of the two arms lie in orthogonal subspaces (Ames, Churchland, 2019; Heming, Cross, Takei, Cook & Scott, 2019). These hypotheses are not mutually exclusive: For example, the degree of overlap or independence may depend on the gesture type (e.g., overlapping representations for grasping but not arm movement, Downey et a., 2020), or brain region (e.g., premotor cortex displays stronger preservation of tuning preferences across the two arms than primary motor cortex, Cisek, Crammond & Kalaska, 2003).

One factor that has received little attention in this literature is the recording hemisphere. This is surprising given the marked asymmetries between the two hemispheres in terms of praxis (Corballis, Badzakova-Trajkov & Häberling, 2012; Rothi, Ochipa & Heilman, 1997). Tracing back to the early 20th century, marked hemispheric asymmetries have been defined by the behavioral deficits observed following unilateral brain injury (Schaefer, Haaland & Sainburg, 2007; Liepmann 1908, cited in Renzi, & Lucchelli, 1988). Apraxia, an impairment in the production of coordinated, meaningful movement in the absence of muscle recruitment deficits, is much more common after left compared to right hemisphere insult (Haaland, Harrington & Knight, 2000; Renzi, & Lucchelli, 1988). Moreover, left hemisphere stroke will frequently result in apraxic symptoms for gestures produced with either hand, as well as impairments in action comprehension (Renzi, & Lucchelli, 1988). Hemispheric asymmetries are also evident in neuroimaging activation patterns in healthy participants, with the left hemisphere having stronger activation during ipsilateral movement than the right hemisphere, especially with increasing task difficulty (Chettouf et al., 2020, Verstynen et al. 2005; Verstynen and Ivry

2011; Schäfer et al, 2007). These patterns raise the possibility that the ipsilateral cortical representation differs between the left and right hemispheres.

In the present study, we use intracranial recordings from the cortical surface (ECoG) to examine the degree of cortical overlap for ipsilateral and contralateral upper limb movement in the left and the right hemisphere. The data were collected from six patients, three with left hemisphere implants and three with right hemisphere implants, while they engaged in an instructed-delay reaching task. We focus on predicting the temporal dynamics of high frequency activity (HFA; 70-200Hz), a surrogate for infragranular single-unit activity and supragranular dendritic potentials, (Leszczynski et al., 2020) which tracks local activation of the cortex (Muthukumaraswamy, 2010). Going beyond previous studies that use decoding models which combine multiple neural features from multiple electrodes to predict kinematics, we employed an encoding model which uses kinematic features to predict neural activity for each electrode, allowing us to retain the high spatial and temporal resolution of the ECoG signal. This approach allows us to create high-resolution topographic maps depicting encoding strength on the surface of the cortex for movements produced with the contralateral and ipsilateral arm. This is preferable to projecting the weights obtained from decoding models since these models have difficulty disambiguating between informative and uninformative electrodes (Kriegeskorte & Douglas, 2019). Moreover, our approach provides a way to map kinematics to neural activity in a time-resolved manner (rather than as single weights), allowing us to identify time ranges of representational overlap and divergence across the two arms for each electrode.

RESULTS

Behavior. Patients made continuous reaches to and from the touchscreen, producing roughly, bell-shaped velocity profiles for both the outbound and the inbound segments of our estimated kinematics (Fig 1C,1E). Table 1 summarizes the total number of successful trials, along with the reaction time and movement time data. A trial was considered unsuccessful if the reach was initiated before the go cue or if contact with the touchscreen was outside the boundary of the target. The percentage of unsuccessful trials was low, ranging between 0% to 12.5% across individuals. Outbound reaches (platform to touchscreen) were, on average, faster than inbound reaches (touchscreen to platform) for the majority of patients. Note that the reaction time data are averaged across left and right arm reaches since there was no consistent difference on this measure.

Patient ID	Handedness	RT	Outbound reach	Inbound reach	Total trials
L1	Right	392 (102)	703 (118)	907 (287)	152
L2	Right	1574 (871)	598 (173)	1003 (406)	146
L3	Ambidextrous	771 (345)	946 (183)	1429 (252)	148
R1	Right	518 (194)	940 (211)	1027 (345)	132
R2	Right	335 (55)	602 (94)	590 (120)	145
R3	Right	534 (157)	721 (145)	1017 (318)	145

Table 1. Summary of performance measures for each participant.

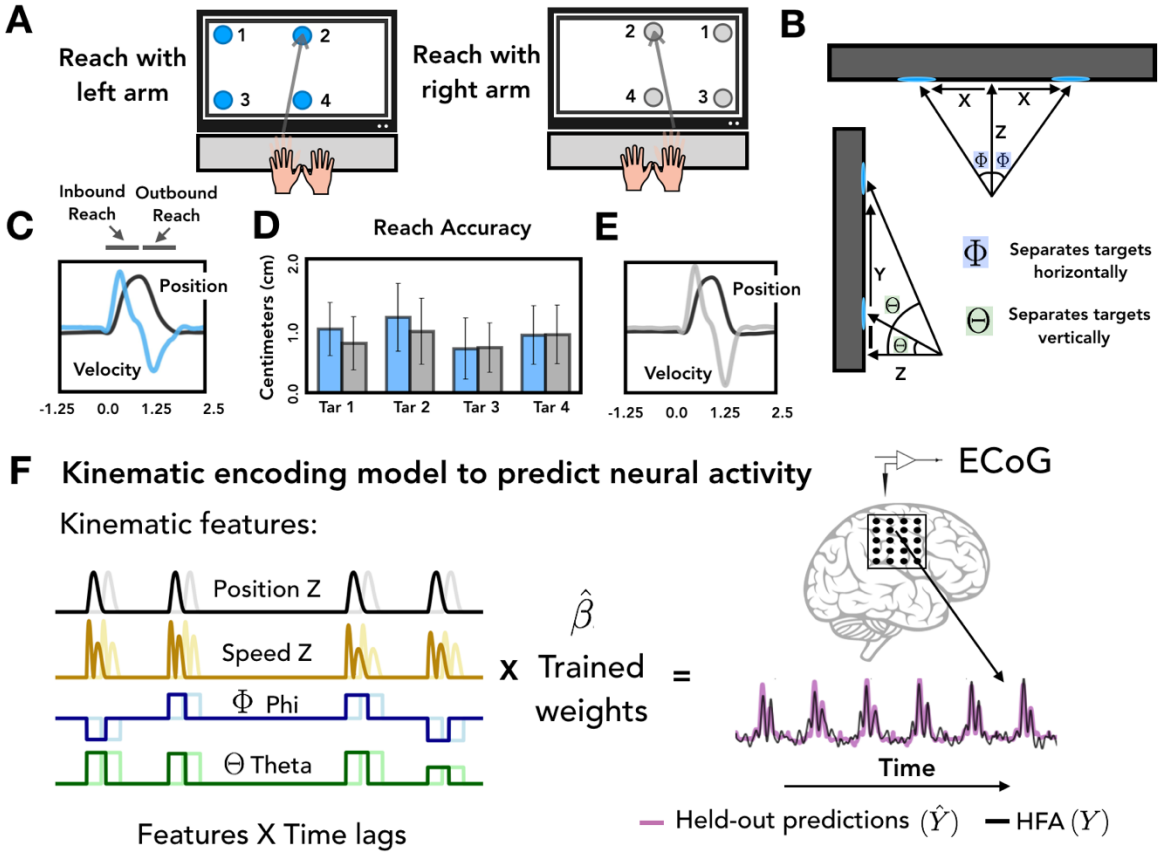

Figure 1. Task and model design. A) Task design. Patients performed an instructed-delay reaching task, moving to targets that appeared on a touchscreen monitor with either the left or right arm. **B) Task Schematic.** Target position with respect to the start position of the reaching arm can be defined on the basis of three Cartesian coordinates (X, Y, Z) and two spherical angles (Theta and Phi). **C) Reaching profile, left.** Average estimated position and velocity traces for a representative series of trials performed with the left arm. **D) Reach accuracy.** Accuracy was quantified as the absolute distance from the center of each target (target diameter = 2.5cm) to the touch location for all four targets with the left (blue) and right (grey) arm. **E) Reaching profile, right.** Same as C, but with the right arm. **F) Kinematic encoding model**. Time lagged estimated kinematic features were used to the predict high frequency activity (HFA) for each electrode using ridge regression. Four kinematic features were included in the model: Position in the Z dimension, speed in the Z dimension and the two spherical angles Phi and Theta. Kinematic features were trained on a subset of the HFA data and predictions of HFA activity were evaluated with held-out test sets.

At a more fine-grained level of spatial accuracy, we calculated the distance from the center of each target to the touch location for each trial. On average, the mean distance from the center of the 2.5 cm circle was 0.80 cm (*SD* = 0.10 cm) for right-handed reaches and 0.90 cm (*SD* = 0.17 cm) for left-handed reaches (Fig 1D). These values did not differ from one another (t = 1.538, p = .222).

Stronger bilateral encoding in the left hemisphere. We examined the extent to which movement kinematics were encoded for contralateral and ipsilateral reaches in individual electrodes. To do this we fit a kinematic encoding model that maps continuous kinematic features to the HFA signal (Fig 1F) for the 665 electrodes meeting

our inclusion criteria. This procedure was done separately for contralateral and ipsilateral reaches. We quantified the cross-validated model fit by generating HFA predictions using the kinematic features from held-out trials of the same condition and calculating prediction performance as the square of the linear correlation (R^2) between the predicted and actual HFA signal (Fig 2B).

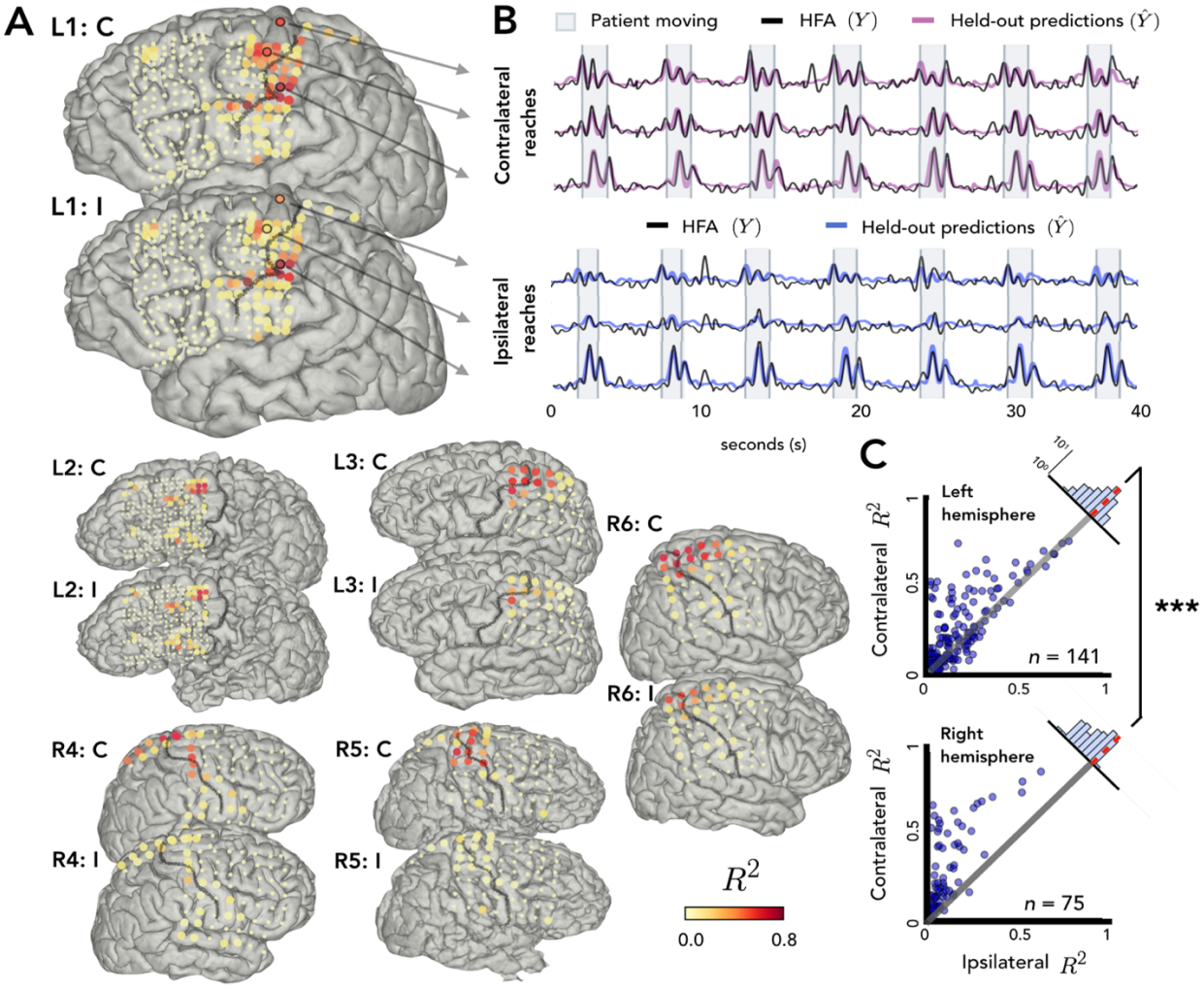

Figure 2. Stronger bilateral encoding in left hemisphere. Held-out prediction performance (R^2) was computed for each electrode during contralateral reaches (C) and ipsilateral reaches (I). R^2 was calculated as the squared linear correlation between the actual HFA and the predictions based on the model. **A) Prediction performance maps for individual patients.** Performance of each electrode, shown at the idiosyncratic electrode location for each participant (location based on clinical criteria). Electrodes that did not account for at least .05% of the variance (R^2 <.05) in either the contralateral or ipsilateral condition are shown as smaller dots. **B) Model predictions.** Representative time series of the actual HFA and model-based predictions for three electrodes during contralateral and ipsilateral reaches**. C) Summary across patients.** Scatter plot displaying R^2 values separately for patients with electrodes in either the left (upper) or right (lower) hemisphere. R^2 for contralateral predictions are plotted against R^2 for ipsilateral predictions. Electrodes close to the unity line encode both arms equally whereas electrodes off the unity line indicate stronger encoding of one arm. Points above the unity line indicate stronger encoding of the contralateral arm. These differences are summarized in the frequency histograms in the upper right of each panel. The histogram shows less of a shift in the left hemisphere, a signature consistent with stronger bilateral encoding. *p<0.05, **p<0.01, ***p<0.001, permutation test.

Figure 2A displays R^2 values for each electrode for the contralateral and ipsilateral condition, presented on the individual patient MRIs. Electrodes with high prediction performance were primarily located in arm areas of sensorimotor cortex. In line with previous research (Downey et a., 2020), a sizeable percentage of the electrodes were able to predict the HFA at or above our criterion of $R^2 > .05$ (examples shown in Figure 2B). This degree of prediction was observed not only when the data were restricted to contralateral movement (31% of electrodes), but also when the data were from ipsilateral movement (25%). A number of electrodes (24%) were predictive in both the contralateral and ipsilateral models. Electrodes that did not meet this criterion for either arm are represented as small dots in figure 2A and were excluded from further analysis, leaving a total of 216 predictive electrodes (32%, 141 = left hemisphere, 75 = right hemisphere).

We next asked whether prediction was stronger for contralateral movement, and whether this varied between the two hemispheres. Figure 2C compares the predictive performance for each electrode for the contralateral and ipsilateral conditions. Values close to the unity line yield similar predictions for the conditions; values off the unity line indicate that encoding is stronger for one arm compared to the other. To compare prediction performance at the group level, distributions were created by taking the difference between the R^2 values for the contralateral and ipsilateral conditions for each electrode (Figure 2C, upper right corner of each scatterplot). As can be seen, there is a pronounced contralateral bias for both hemispheres (one sample t-test against zero: $\Delta R^2_{\text{left}} = 0.024$, $p_{\text{left}} < .001$, $\Delta R^2_{\text{right}} = 0.115$, $p_{\text{right}} < .001$). Importantly, the contralateral bias was attenuated in the left hemisphere compared to the right hemisphere (permutation test, $p < .001$), indicating stronger bilateral encoding in the left hemisphere. In addition to the hemisphere effect, we also found that the contralateral bias becomes weaker the further the electrodes are from putative primary motor cortex in both hemispheres ($r_{\text{left}} = -0.48$, $p_{\text{left}} < .001$, $r_{\text{right}} = -0.45$, $p_{\text{right}} < .001$; Fig S2).

Opposing patterns of kinematic encoding for the left and right hemisphere during planning and execution. As neural activity unfolds from preparation to movement, the underlying computations may change substantially (Elsayed et al., 2016). To examine if hemispheric asymmetries in encoding depend on task state, we repeated the analysis described in the previous section, but now separated the data to test the held-out predictions during the instruction and movement phases (Fig 3A). We used a mixed design permutation test to examine the effect of hemisphere and task phase on our measure of contralateral bias (Fig 3B).

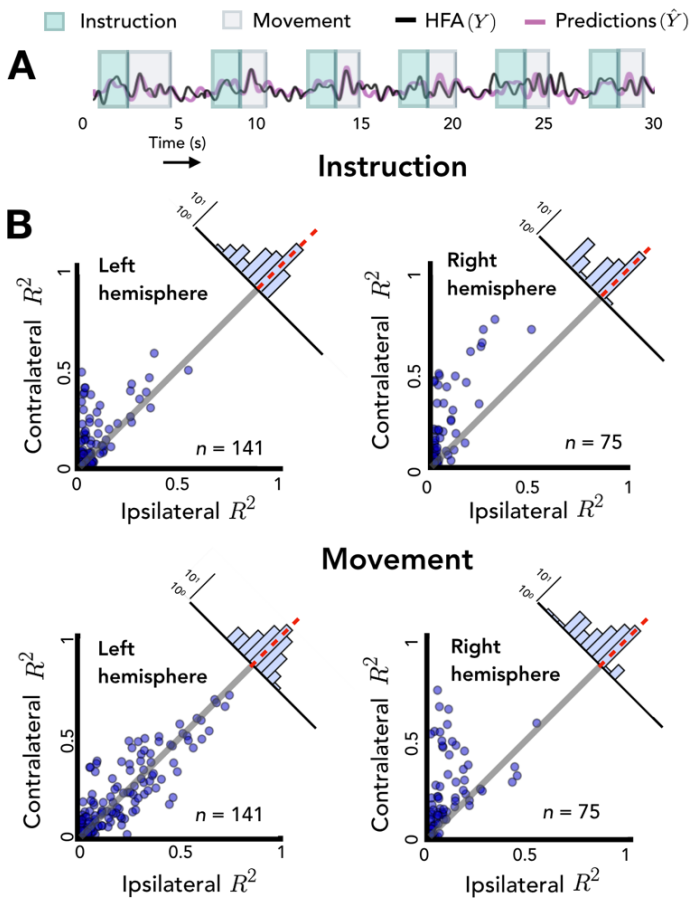

Figure 3. Opposing encoding patterns for left and right hemisphere across task phase. For all predictive electrodes the time series was segmented into instruction and movement epochs. R^2 was then calculated separately for each epoch. **A) Example model predictions.** Time series of a representative electrode with boxes surrounding the instruction (teal) and movement epochs (grey). **B) Prediction performance during movement and instruction.** Comparison of R^2 values for contralateral and ipsilateral predictions during the instruction epoch (top) and the movement epoch (bottom) for patients with electrodes in the left hemisphere (left) or right (right) hemisphere. Bilateral encoding was stronger in the left hemisphere, an effect that was especially pronounced during the movement phase.

As in the previous analysis, the effect of hemisphere was significant, with stronger bilateral encoding (i.e., smaller difference score) in the left hemisphere compared to the right hemisphere ($p < .001$). The effect of task phase was not significant, but there was a significant interaction between hemisphere and task phase ($p < .005$): There was a larger difference between the two hemispheres during the movement phase compared to the instruction phase. Analyzing simple effects within each hemisphere, we found that encoding in the left hemisphere was more bilateral during movement compared to instruction ($\Delta R^2_{\text{left\_move}} = 0.006$, $\Delta R^2_{\text{left\_instruction}} = 0.042$, $p < .001$). In contrast, the opposite pattern was observed in the right hemisphere, with encoding being more bilateral during the instruction phase ($\Delta R^2_{\text{right\_move}} = 0.127$, $\Delta R^2_{\text{right\_instruction}} = 0.103$, $p < .001$). The contralateral bias was most attenuated in the left hemisphere during the movement condition, with a mean difference score that was not statistically different from zero ($p_{\text{left\_move}} = .482$). For the left hemisphere instruction phase and both phases for the right hemisphere, the contralateral bias was significant ($p_{\text{left\_instruction}} < .001$, $p_{\text{right\_move}} < .001$, $p_{\text{right\_instruction}} < .001$). These results suggest that the left and right hemisphere may have different roles in bilateral encoding with regard to task phase. In particular, the contralateral bias disappears in the left hemisphere during movement indicating that prediction performance was not different for movements produced with either the contralateral or ipsilateral arm.

Across arm generalization: More overlap between arms in the left hemisphere. The preceding analyses focused on an encoding analysis for within-arm prediction. We next evaluate the overlap between the neural representations for contralateral and ipsilateral movement. To this end, we examined across-arm prediction performance by

training the kinematic encoding model with the data from movements produced with one arm and testing prediction performance using the data from movements produced with the other arm.

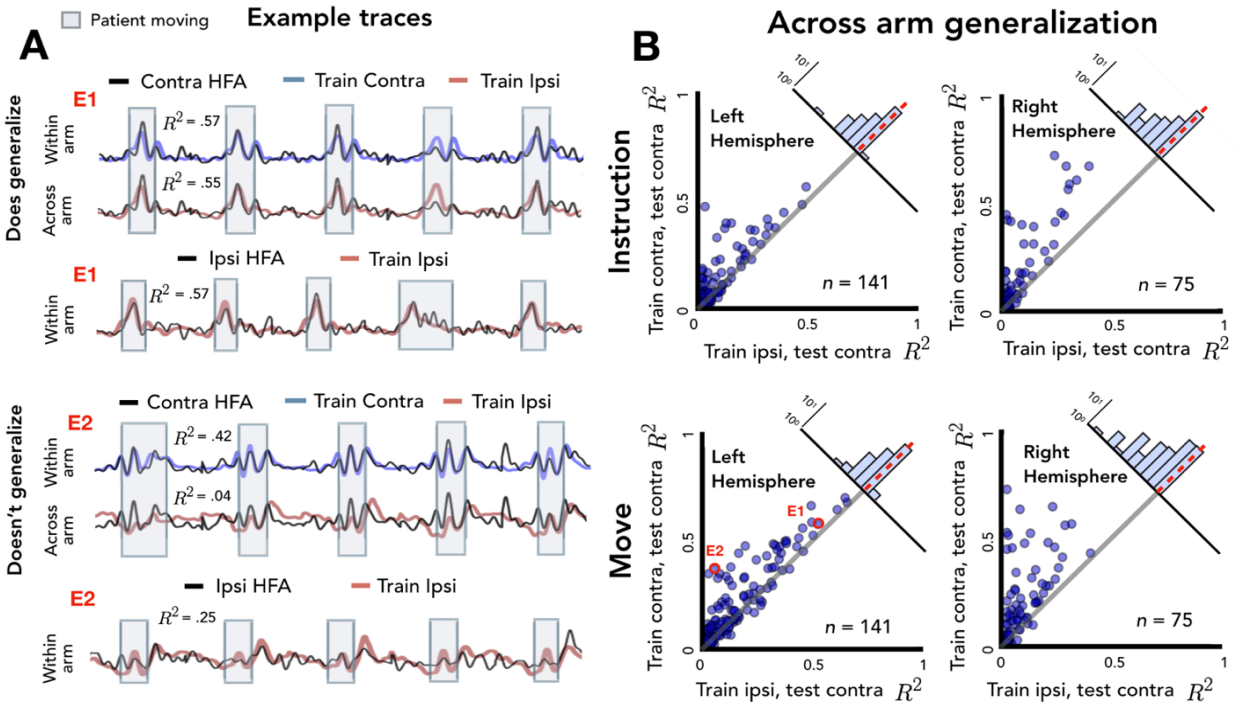

Figure 4. Stronger across-arm generalization in the left hemisphere. Across-arm predictions were created by training the model on ipsilateral reaches and using the trained weights to predict HFA during contralateral reaches. (Within-arm predictions generated the same as in Figs 2 and 3.) Electrodes close to the unity line have overlapping neural representations across the two arms whereas electrodes off the unity line indicate that the two arms are being encoding differentially. **A) Model Predictions.** Predicted and actual HFA for two electrodes selected from the distribution of left-hemisphere electrodes during movement, one that generalizes well across arms (E1) and one that fails to generalize (E2). Bottom row shows within-arm performance for ipsilateral trials, demonstrating that the failure to generalize across arms does not necessarily indicate poor ipsilateral performance. **B) Across-arm generalization across patients.** R^2 for within-arm predictions plotted against R^2 for across-arm predictions, with the analysis performed separately for the instruction and movement phases. Left hemisphere electrodes showed better generalization than right hemisphere electrodes, an effect that was magnified in the movement phase.

Figure 4A shows the traces for two representative electrodes, one that shows good generalization across the two arms and the other that shows poor generalization. For the electrode that shows good generalization (E1), prediction performance for held-out contralateral reaches is comparable when the model is trained on data from either the contralateral or ipsilateral arm. This suggests that there is overlap between the neural representations for reaches performed with either upper limb for this electrode. In contrast, the electrode showing poor generalization (E2) showed good prediction for contralateral reaches when trained with contralateral data, but poor prediction when trained with ipsilateral data. Here the neural representations for the arms do not overlap. Note that E2 showed relatively strong within-arm ipsilateral encoding (R^2 = .25); thus, the inability of this electrode to generalize across arms is not a result of poor encoding of the ipsilateral arm. Rather, E2 encodes movement produced by either arm, but the manner in which they are encoded differs.

Figure 4B summarizes the comparison of within-arm prediction (y axis) against across-arm prediction (x axis), with the data separated for the instruction and movement phases. In this depiction, electrodes close to the unity line have overlapping neural representations during contra- and ipsilateral movement, whereas electrodes off the unity line encode the two arms differentially. We again used a mixed design permutation test, now applied to the difference between within-arm R^2 and across-arm R^2 for each electrode (Figure 4B, upper right corner of each scatterplot). Overall, the left hemisphere showed stronger between-arm generalization than the right hemisphere (main effect of hemisphere: $\Delta R^2_{\text{left}} = 0.041$, $\Delta R^2_{\text{right}} = 0.108$; $p < .001$). This indicates that the left hemisphere not only has stronger bilateral encoding (Figure 3B) but also has more similar neural representations across the two upper limbs. We also found a main effect of task phase, with better across-arm generalization occurring during instruction compared to movement (main effect of task phase: $\Delta R^2_{\text{instruction}} = 0.050$, $\Delta R^2_{\text{movement}} = 0.079$; $p < .001$).

In addition to these main effects, there was also a significant interaction between task phase and hemisphere ($p < .05$). Analyzing simple effects within each task phase, the left hemisphere had better across-arm generalization for both the instruction and movement phase (simple effect analysis: $p_{\text{instruct}} < .001$, $p_{\text{move}} < .001$). In addition, better across-arm generalization was found during the instruction phase in both the left and the right hemispheres (simple effect analysis: $p_{\text{left}} < .001$, $p_{\text{right}} < .001$). The significant interaction indicates that while the neural representations across arms became more distinct in both hemispheres with the transition from instruction to movement, this difference was more pronounced in the right hemisphere. In sum, electrodes in the left hemisphere generalize across-arms better during instruction and movement compared to the right hemisphere and electrodes in the left hemisphere also change less during the transition from instruction to movement compared to the right hemisphere.

Temporal and spatial topography of across-arm generalization. To examine how generalization varied across the cortex, we categorized each electrode as showing either good across-arm generalization (decrease of up to 20% relative to within-arm performance) or poor across-arm generalization (decrease of more than 50%; Fig 5A). We focused on the extremes of the generalization distribution based on the assumption that these electrodes were more likely to share similar underlying neural profiles. This also allowed us to have similar numbers of electrodes in each group.

As can be seen in Figure 5B, electrodes that generalize well were predominantly found in the left hemisphere (white circles). In contrast, electrodes showing poor generalization are observed in both hemispheres (magenta circles). Moreover, in both hemispheres, electrodes showing poor generalization were clustered near the dorsal portion of the central sulcus, a region corresponding to the arm area of motor cortex. Electrodes showing strong generalization (mostly limited to the left hemisphere) tended to be in dorsal and ventral premotor cortices, along with a few in dorsal parietal lobe. This pattern was also observed when we analyzed all electrodes, rather than restrict the analysis to those showing extreme values. Here we used continuous measures, correlating the amount of across-arm generalization with the distance (absolute value) from the dorsal aspect of the central sulcus. The correlation was significant in the left hemisphere ($r_{\text{left}} = 0.463$, $p_{\text{left}} < .001$) but did not reach significance in the right

hemisphere, although the trend was in the same direction (r_{right} = 0.224, p_{right} = .068; Fig S2).

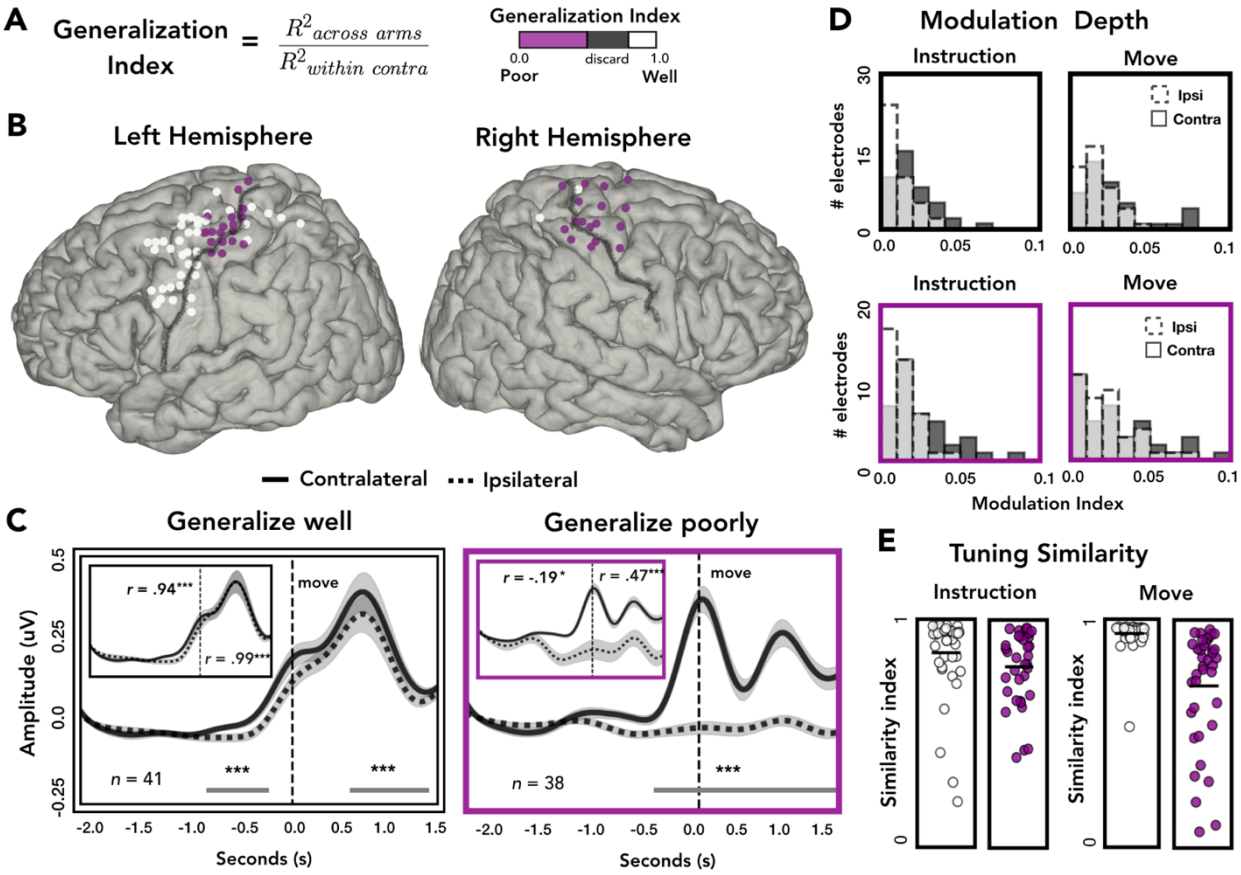

Figure 5. Spatial and temporal relationship of across-arm generalization. A) Generalization index. Electrodes were classified as showing good across-arm generalization (white, generalization index > .80) or poor across arm generalization (magenta; generalization index < .50). **B) Spatial distribution of across-arm generalization.** Electrodes that generalize well across arms (white) were primarily located in dorsal and ventral premotor regions of the left hemisphere. Electrodes that generalize poorly (magenta) were clustered around the putative arm area of the central sulcus in both the left and right hemispheres. **C) Amplitude differences across arms.** Average contralateral (solid line) and ipsilateral (dashed line) predictions for electrodes that generalize well across arms (left) or generalize poorly (right). Significant clusters are represented with a gray line. Inset: Same data but standardized to highlight shape of the timeseries independent of absolute amplitude**. D) Modulation depth.** Depth of tuning was calculated during instruction or movement with either the ipsilateral or contralateral hand. Greater modulation was found during contralateral reaches and during movement. **E) Tuning similarity.** Across arms tuning similarity was calculated for electrodes that generalize well (white) or poorly (magenta). Electrodes that generalize well across arms had significantly more tuning similarity than electrodes that did not generalize. *p<0.05, **p<0.01, ***p<0.001, cluster permutation test, Pearson's correlation.

To examine the dynamics of representational overlap and divergence, we averaged the time-resolved HFA amplitude across electrodes, restricted to those included in the categorical analysis. Figure 5C displays the average time series for contralateral (solid line) and ipsilateral (dashed line) predictions for electrodes that generalize well (white) or poorly (magenta). The temporal profile of HFA activity is similar for electrodes that generalize well, showing a single peak in the movement phase. A cluster-based permutation test identified two periods where the HFA amplitude

differed for contralateral and ipsilateral reaches, one during instruction and one well into the movement period. In contrast, the temporal profiles are radically different for those that generalize poorly, primarily because of the weak modulation during ipsilateral reaches. Interestingly, these electrodes also showed a double-peaked temporal profile during contralateral reaches. Similar multi-phasic activity has been observed in single unit activity in M1 during reaching (Churchland et al., 2012).

It is possible that similarity in temporal structure is obscured in the preceding analysis by the differences in HFA amplitude for the electrodes that showed poor generalization. To control for this, we standardized the time series data by dividing each sample by the overall standard deviation (Insets: Fig 5C). Using the standardized traces, we calculated the linear correlation coefficient between the contralateral and ipsilateral traces, separately for instruction and movement. As expected, electrodes that generalized well across arms showed strong across-arm correlations for both task phases (Inset Fig 5C, *left*). In contrast, for electrodes that generalize poorly across arms, the correlation between arms was negative during instruction and then rose to a moderate positive correlation during movement (Inset Fig 5C, *right*). Thus, the poor generalization of these electrodes is generally due to the temporal divergence of the two arms during instruction, where the ipsilateral trace becomes inhibited compared to the contralateral trace. Interestingly, although the ipsilateral trace remains inhibited during movement, the temporal structure between the two arms re-emerges.

Target modulation and tuning similarity across arms. To examine the extent of target modulation for the contralateral and ipsilateral arm, we calculated the modulation depth of each electrode during the instruction and movement phases. The modulation index reflects the amount of variability in the signal captured by target tuning (or target specificity): A modulation index of .1 means 10% of the variance is captured by the difference between the response to the four target locations. The modulation values overall were relatively low (Fig 5D). However, it should be noted that the reaches were all within the fronto-parallel plane which comprise a considerably smaller range of movement compared to studies that use a center-out reaching task. For both electrode types (showing good or poor across arm generalization), there was a main effect of arm, with ipsilateral modulation lower than contralateral modulation ($p_{Generalize\_well} < .001$; $p_{Generalize\_poorly} < .005$). Both subgroups of electrodes also displayed a main effect of task phase, with the depth of modulation greater during the movement phase compared to the instruction phase ($p_{Generalize\_well} < .001$; $p_{Generalize\_poorly} < .005$). No significant interactions were found for either group.

We also examined the representational overlap between the two arms in terms of their tuning profiles. We computed a tuning similarity index, defined as the sum of squared errors for average HFA predictions to the same target between the contralateral and ipsilateral arms. A similarity index of 1 would correspond to identical tuning preferences for the arms whereas a similarity index of 0 would indicate completely disparate tuning preferences. The similarity data were analyzed with a mixed design permutation test, including the factors task phase and electrode type (good vs. poor generalizers). Electrodes that generalize well across the two arms (predominately found in the left hemisphere) showed more overlap of tuning preferences compared to electrodes that generalized poorly (main effect of generalizability: $p < .001$). While there was no effect of phase ($p = .758$), the interaction was significant ($p < .005$), with electrode types showing more comparable tuning similarity during instruction and tuning similarity diverging during movement. Simple

effects analysis revealed that for electrodes that generalize poorly, tuning similarity was higher during the instruction phase compared to the movement phase ($p < .001$). In contrast, for electrodes that generalize well, tuning similarity was higher during movement compared to instruction ($p < .001$). These analyses demonstrate that a number of electrodes in the left hemisphere strongly encode kinematic variables for both arms, including similar tuning preferences across the two arms, which was especially pronounced during the movement phase.

DISCUSSION

Although the most prominent feature of cortical motor pathways is their contralateral organization, unimanual movements are well represented in the ipsilateral hemisphere. Single-unit activity and local field potentials obtained from motor cortex in non-human primates (Ganguly et al., 2009; Ames & Churchland, 2019), as well as ECoG activity in humans (Bundy, Szrama, Pahwa & Leuthardt, 2018; Ganguly et al., 2009, Wisneski et al., 2008) can be decoded to predict complex kinematic variables and EMG activity during arm movements of the ipsilateral arm. Here we extend this work by building a kinematic encoding model to examine how these features are represented in each hemisphere. We opted to build an electrode-wise encoding model which opened up new avenues for analysis. Electrode-wise encoding models allow prediction of the full time series for each electrode thus retaining the high spatial and temporal resolution of the intracranial signal. From these metrics we could compare kinematic encoding and across-arm generalization between the two hemispheres as well as the spatial distribution of the information-carrying electrodes within each hemisphere. We observed a marked hemispheric asymmetry: While contralateral movements were encoded similarly across the two hemispheres, ipsilateral encoding was much stronger in the left hemisphere, an effect that was especially pronounced during movement execution. In addition, there was greater overlap between the representation of contra- and ipsilateral movement in the left hemisphere compared to the right hemisphere.

Hemispheric asymmetry in movement encoding. We observed a striking asymmetry between the two hemispheres for ipsilateral movement encoding, with stronger bilateral encoding of the upper limbs in the left hemisphere compared to the right hemisphere. The effect size is quite substantial (d = 1.34), which exceeds Cohen's (1988) convention for a large effect (d = .80). We studied three patients per hemisphere, with each patient having at least 17 predictive electrodes, totaling 141 electrodes in the left hemisphere and 75 in the right hemisphere.

Given the size of the hemispheric asymmetry effect, it is surprising that this asymmetry has not be described in previous reports. This may in part reflect the smaller sample size in these studies. For example, in Bundy et al. (2018), three of the four patients had left hemisphere grids, leaving a hemisphere analysis dependent on the data from a single right hemisphere patient. Studies with non-human primates tend to ignore hemispheric differences, perhaps because these animals do not show consistent patterns of hand-dominance across individuals. One exception here is a study by Cisek, Crammond and Kalaska (2003) who reported no hemispheric differences in neural recordings obtained from M1 and PMd during ipsilateral and contralateral arm reaches.

In addition to examining hemispheric differences in the encoding of unimanual movement, we also asked if kinematic features were encoded differently for contra- and ipsilateral movements by testing across-arm generalization. We categorized electrodes

as showing either good across-arm generalization (decrease of up to 20% relative to within-arm performance) or poor across-arm generalization (decrease of more than 50%). This categorization scheme revealed a striking anatomical division, with electrodes showing good across-arm generalization clustering in the left premotor and parietal cortices and electrodes that generalized poorly clustering in left and right M1. Using the same categorization, we further examined the spatial tuning of the electrodes. Target tuning in the HFA band was found for both contralateral and ipsilateral movement, although ipsilateral tuning was significantly shallower. Interestingly, electrodes that generalized well across-arms had similar target tuning for each arm. This suggests that for these electrodes, ipsilateral signals are not just encoding generic movement, but encoding movement direction in a similar manner to contralateral signals. A similar overlap in tuning has been observed in single unit recordings from PMd (Cisek, Crammond & Kalaska, 2003) and can be inferred from the across-arm generalization decoding results reported by Bundy et al., (2018). In contrast, electrodes that failed to generalize, located primarily in M1 in either left or right hemisphere, exhibited disparate tuning for contra- and ipsilateral reaches.

One limitation of our study is that, because two of the left hemisphere patients had high density grid implants, there were fewer right hemisphere electrodes compared to the left hemisphere electrodes. However, all three right hemisphere patients had coverage over dorsal and ventral premotor cortices, making it unlikely that the poor across-arm generalization for right hemisphere electrodes is due to insufficient coverage.

Functional implications of hemispheric asymmetries in movement encoding. By using a delayed response task, we were able to segregate activity into a instruction phase during which the patient was presented with the target location for the forthcoming movement and a movement phase, defined at the onset of the reach. With this design, we found that the encoding model could predict neural activity during the instruction phase based on the kinematics of the forthcoming reach, evidence that the patients were indeed planning the upcoming movement.

This task phase analysis also revealed robust asymmetries between the two hemispheres. There was a main effect of hemisphere, with the left hemisphere displaying stronger bilateral encoding overall compared to the right hemisphere. However, there was also an interaction: In the left hemisphere bilateral encoding was stronger during the movement phase whereas in the right hemisphere bilateral encoding was stronger during the instruction phase. Surprisingly, in the left hemisphere the contralateral bias completely disappeared during the movement phase, with both the contra- and ipsilateral arms being encoded to the same extent. Stronger bilateral encoding during movement (compared to instruction) is surprising given the spatial distribution of electrodes that encode ipsilateral movement were primarily outside of M1, regions typically associated more with planning than execution (e.g., premotor cortices, parietal cortex).

The asymmetry observed here is in accord with the long-standing recognition of hemispheric asymmetries in praxis. Starting with the classic observations of Liepmann at the turn of the 20th century on the association of the left hemisphere and apraxia (Liepmann 1908, cited in Renzi, & Lucchelli, 1988; see also Schaefer et al., 2007) and continuing with functional imaging studies in neurotypical populations, a large body of evidence points to a dominant role for the left hemisphere in skilled movement often

engaging bi-manual movements (Corballis, Badzakova-Trajkov & Häberling, 2012; Przybylski & Króliczak, 2017). This asymmetry is most pronounced in tasks involving functional object use (Buxbaum et al., 2006), symbolic gestures (Xu, Gannon, Emmorey, Smith & Bruan, 2009) and intransitive pantomimes (Bohlhalter et al., 2009). Apraxia, following left-hemisphere damage can be manifest in movements produced with either limb (Renzi, & Lucchelli, 1988), and are usually associated with lesions that encompass premotor and parietal cortices (Haaland, Harrington & Knight, 2000). While this asymmetry may be linked to hand dominance (Ochipa, Rothi & Heilman, 1989), functional imagining studies with relatively large sample sizes have shown that handedness only influences the strength of the left hemisphere bias for skilled movement but does not produce a reversal in left handers (Vingerhoets et al., 2012; Verstynen et al., 2005, Chettouf et al., 2020, Vingerhoets et al., 2013). Of the six patients tested in the current study, five are right-handed and the remaining patient reported being ambidextrous with a slight preference for using the left hand. We note that the results from this patient (L3) did not qualitatively differ from the other two left hemisphere patients.

Ipsilateral encoding was most prominent in the premotor and parietal cortex of the left hemisphere, overlapping with the neural regions implicated in praxis. However, two features of our results do not map on readily to an interpretation that focuses on hemispheric asymmetries in praxis. First, our task involved simple reaching movements, whereas praxis generally encompasses more complex learned movements associated with tool use or symbolic gestures. Second, ipsilateral encoding became more pronounced during movement execution; a priori, one might have expected this asymmetry to be more related to gestural intent and thus be more prevalent during movement planning.

An alternative hypothesis is that the ipsilateral activation is reflective of a prominent role of the left hemisphere in bimanual coordination. The encoding of ipsilateral arm movement might be a form of state representation, a means to keep track of the state of the ipsilateral arm given that many actions require the coordinated activity of the two limbs. This hypothesis, derived from the current data, is consistent with the increased ipsilateral encoding during the movement phase. The need to monitor the state of the other limb should hold for unimanual gestures performed with either limb. There is evidence in the neuropsychological literature pointing to a role of the left hemisphere in bimanual coordination in neuroimaging (Jäncke et al., 2000; Toyokura, Muro, Komiya & Obara, 1999; Maki, Wong, Sugiura, Ozaki & Sadato, 2008) and electrophysiological studies (Serrien, Cassidy & Brown, 2003). For example, Schaffer et al., (2020) observed greater impairments in bimanual coordination following left hemisphere stroke compared to right hemisphere stroke. Interestingly, the impairment was manifest prior to peak velocity, a finding interpreted as a disruption in predictive control. It may be that the left hemisphere makes an asymmetric contribution to inter-limb coordination by tracking or predicting where both limbs are in space.

An important question for future work is to examine how ipsilateral representations in the left hemisphere are affected during more complex movements, including those that involve both limbs. Using fMRI, Diedrichsen, Wiestler and Krakauer (2013) compared ipsilateral movement representations during unimanual and bimanual movements. Within the primary motor cortex, ipsilateral representations could only be discerned during unimanual movement. However, caudal premotor and anterior parietal regions retained similar ipsilateral representation during uni- and bimanual movement.

If the left hemisphere tracks both limbs to facilitate bimanual coordination, we would predict that ipsilateral representations in premotor cortex are retained more strongly in the left hemisphere compared to the right hemisphere when both arms are engaged in the task.

Conclusion: Using a kinematic encoding model, we observed a striking hemispheric asymmetry, with the left hemisphere more strongly encoding the ipsilateral arm than the right hemisphere, a finding that was apparent during preparation and amplified during movement. This asymmetry was primarily driven by electrodes positioned over premotor and parietal cortices, with strong contralateral encoding for electrodes positioned over sensorimotor cortex. One possible interpretation of our results is that these networks monitor the state of each arm, a prerequisite for most skilled actions.

METHOD

Participants. Intracranial recordings were obtained from six patients (2 female; 5 right-handed) implanted with subdural grids as part of their treatment for intractable epilepsy. Data were recorded at three hospitals: University of California, Irvine (UCI) Medical Center (n = 2), University of California, San Francisco (UCSF) Medical Center (n = 2) and California Pacific Medical Center (CPMC), San Francisco (n = 2). Electrode placement was solely determined based on clinical considerations and all procedures were approved by the institutional review boards at the hospitals, as well as the University of California, Berkeley. All patients provided informed consent prior to participating in the study.

Behavioral task. Patients performed an instructed-delay reaching task while sitting upright in their hospital bed. The patient rested their arms on a horizontal platform (71 cm x 20 cm) that was placed over a standard hospital overbed table. The platform contained two custom-made buttons, each connected to a microswitch. At the far end of the platform (13 cm from the buttons, approximately 55 cm from the patient's eyes), a touchscreen monitor was attached, oriented vertically. Visual targets could appear at one of six locations, four for each arm (Figure 1a). The two central locations were used as targets for reaches with either arm; the two eccentric targets varied depending on the arm used. Stimulus presentation was controlled with Matlab 2016a. A photodiode sensor was placed on the monitor to precisely track target presentation times. The analog signals from the photodiode and the two microswitches were fed into the ECoG recording system and were digitized into the same data file as the ECoG data with identical sampling frequency.

Testing of the contralateral and ipsilateral arms (relative to the ECoG electrodes) was conducted in separate experimental blocks that were counterbalanced. To start each trial, the patient placed their left and right index fingers on two custom buttons to depress the microswitches (this indicated they were in the correct position and ready to start the trial). If both microswitches remained depressed for 500 ms, a fixation stimulus was presented in the middle of the screen for 750 ms, followed by the target, a circle (1.25 cm diameter) which appeared in one of the four locations. Another hold period of 900 ms followed in which the participant was instructed to prepare the required movement while the target remained on the screen. If the microswitch was actuated during this hold period, an error message appeared on the screen and the program would advance to the next trial. If the start position was maintained, a compound imperative stimulus was presented at the end of the hold period. This consisted of an

auditory tone and an increase in the size of the target (2.5 cm diameter). The participant was instructed that this was the signal to initiate and complete a continuous out-and-back movement, attempting to touch the screen at the target location before returning back to the platform. The target disappeared when the touchscreen was contacted. The imperative was withheld on 5% of the trials ('catch' trials) to ensure that the participant only responded after the onset of the imperative.

Once back at the home position, the screen displayed the word 'HIT' or 'MISS' for 750 ms to indicate if the touch had occurred within the target zone. The target zone included the 2.5 diameter circle as well as a 1cm buffer around the target. After the feedback interval, the screen was blank for 250 ms before the reappearance of the fixation stimulus, signaling the start of the next trial. The patients were informed to release either of the buttons at any time they wished to take a break.

Each block consisted of 40 trials (10/target), all performed with a single limb. Blocks alternated between contra- and ipsilateral arms (relative to the ECoG electrodes), with the order counterbalanced across patients. Each block took approximately 5-6 minutes to complete. All patients completed at least two blocks with each per arm (Table 1).

Movement analysis and trajectory reconstruction. We used two methods to analyze the movements. For the first method, we recorded key events defined by the release of the microswitch at the start position, time and location of contact with the touchscreen, and return time to the home position, defined by the time at which they depressed the home position microswitch. For the second method, we used the Leap Motion 3-d movement analysis system (Weichert, et al., 2013) to record continuous hand position and the full movement trajectory (sampling rate = 60 Hz). Although the Leap system is a lightweight video-based tracking device that is highly mobile, the unpredictable environment of the ICU led to erratic recordings from the Leap system. For example, patients frequently had intravenous lines in one or both hands which obstructed the visibility of the hand and interfered with the ability of the Leap system to track the hand using their built-in hand model. This resulted in lost samples and therefore satisfactory kinematic data was obtained from only a subset of conditions collected from patients using the Leap system.

Given the limitations with the Leap data, we opted to use a simple algorithm to reconstruct the time-resolved hand trajectory in each trial, estimating it from the event-based data obtained with the first method. We used a beta distribution to estimate the velocity profile of the forward and return reach based on reach times and the travel distance (sampling rate = 100 Hz). We opted to use a beta distribution because this best matched the velocity profiles of the data obtained with the Leap system.

For conditions that had clean kinematic traces (no lost samples) from the Leap system, we compared the estimated kinematic profiles with those obtained with the Leap system. There was a high correlation between the two data sets (r = .98 for position in the Z dimension; r = .93 for velocity in the Z dimension; Fig S1). We note that our method of estimating the trajectories results in a smoothed version of the movement, one lacking any secondary or corrective movements that are sometimes observed when reaching to a visual target (Suway & Schwartz, 2019). We believe this is still a reasonable estimation given the high correlation with the continuous Leap data, and the fact that participants had ample time to prepare the movements and were

instructed and observed to make ballistic movements by the experimenter who was present for all recording sessions (CMM).

Electrode Localization. Grid and strip electrode spacing was 1 cm in four patients and 4 mm in the two other patients. The electrode locations were visualized on a three-dimensional reconstruction of the patient's cortical surface using a custom script that takes the post-operative computer tomography (CT) scan and co-registers it to the pre-operative structural magnetic resonance (MR) scan (Stolk et al., 2018).

Neural data acquisition and preprocessing. Intracranial EEG data and peripheral data (photodiode and microswitch traces) were acquired using a Nihon Kohden recording system at UCI (128 channel, 5000 Hz digitization) and CPMC (128 channel, 1000 Hz digitization rate), and two Tucker Davis Technologies recording systems at UCSF (128 channel, 3052 Hz digitization rate).

Offline preprocessing included the following steps. First, if the patient's data was not sampled at 1000 Hz (UCI and UCSF recording sites), the signal from each electrode was low-pass filtered at 500 Hz using a Butterworth filter as an anti-aliasing measure before down-sampling to 1000 Hz. Electrodes were referenced using a common average reference. Each electrode was notch-filtered at 60, 120 and 180 Hz to remove line noise. The signals were then visually inspected and electrodes with sustained excessive noise were excluded from further analyses. The signals were also inspected by a neurologist (RTK) for epileptic activity and other artifacts. Electrodes that had pathological seizure activity were also excluded from the main analyses. Out of 752 electrodes, 82 were removed due to excessive noise and 5 were removed due to epileptic activity, resulting in a final data set of 665 electrodes. Catch trials and unsuccessful reaches were not included in the analyses.

From the cleaned data set, we extracted the HFA instantaneous amplitude using a Hilbert transform. To account for the 1/*f* power drop in the spectrum, we divided the broadband signal into five narrower bands that logarithmically increased from 70 to 200 Hz (i.e., 70-86, 86-107, 107-131, 131-162, 162-200 Hz), and applied a band-pass filter within each of these ranges. We then took the absolute value of the Hilbert transform within each band-pass, performed a z-score transformation, and averaged the five values. Z-scoring was performed after concatenating all the blocks for each patient, ensuring that we did not obscure possible amplitude differences across the two arms. As a final step, the data were down-sampled to 100 Hz to reduce computational load (e.g., number of parameters in the encoding model, see below). HFA amplitude fluctuations (envelope; are evident at lower frequencies (Canolty et al., 2006; Pei et al., 2011).

Feature selection. Four estimated kinematic features were used to predict HFA (Figure 1B *left*). The first two features were position and speed in the Z dimension. This dimension captures variability related to movement that is relatively independent of target location (i.e., along the axis between the patient and touchscreen). The second pair of features were spherical angles that define the specific target locations (Figure 1A *right*). Features were selected to reduce collinearity and redundancy in the encoding model. Because we include time lags for each kinematic feature, derivatives can emerge from the linear model (e.g., velocity and acceleration can be created from position); thus, velocity and acceleration were not included as additional features. Speed is a non-linear transformation of position and is added as a separate feature.

Kinematic encoding model. The estimated kinematic features were used to predict the HFA for each electrode (Fig 1F). We created a 4 x 400 feature matrix by generating a time series for each feature by time-lagging the values of the selected feature relative to the neural data, with lags extending from 2 s before movement onset to 2 s after movement onset (sampling rate at 100 Hz). This wide range of lags serves two purposes. First, it provides a way to compensate for the anticipated asynchrony between neural data and movement kinematics. Second, it allowed us to evaluate HFA activity during the instructed delay (beginning ~1.5 s before movement onset) period as well as during movement. HFA at each time point [HFA(t)] was modeled as a weighted linear combination of the kinematic features at different time-lags, resulting in a set of beta weights, b1 …, b400 per kinematic feature. To make the beta weights scale-free, the kinematic features and neural HFA were z-scored before being fit by the model.

Model fitting. Regularized (ridge) regression (Hoerl and Kennard, 1970) was used to estimate the weights that map each kinematic feature (X) to the HFA signal (y) for each electrode, with λ being the regularization hyperparameter:

$$\hat{\beta} = (X^T X + \lambda I)^{-1} X^T y$$

For within-arm model fitting, the total dataset consisted of all clean, successful trials performed with either the ipsilateral or contralateral arm (each arm was fit separately). Nested five-fold cross-validation was used to select the regularization hyperparameter on inner test sets (validation sets) and assess prediction performance on separate, outer test sets. At the outer level, the data was partitioned into five mutually exclusive estimation and test sets. For each test set, the remaining data served as the estimation set. For each outer fold, we further partitioned our estimation set into five mutually exclusive inner folds to train the model (80% of estimation set) and predict neural responses across a range of regularization values on the validation set (20% of estimation set). For each inner fold, the regularization parameter value was selected that produced the best prediction as measured by the linear correlation of the predicted and actual HFA. The average of the selected regularization parameters across the five inner folds was computed and used to calculate the prediction of the HFA on the outer test set. This procedure was done at the outer level five times. Our primary measure is held-out prediction performance (R^2), which we quantified as the squared linear correlation between the model prediction and the actual HFA time series, averaged across the five mutually exclusive test sets.

To be considered as predictive, we established a criterion that an electrode must account for at least 5% of the variability in the HFA signal ($R^2 > .05$) for either ipsilateral or contralateral reaches (Downey et a., 2020). Electrodes not meeting this criterion were not included in subsequent analyses.

For across-arm model fitting, the same procedure was used except the test set was partitioned from the total dataset of the other arm. We partitioned the data in this manner (80% estimation, 20% test) to make the fitting procedure for the across-arm model comparable to that employed in the within-arm model.

Tuning modulation and similarity across arms. Modulation depth of target tuning was calculated as the standard deviation of the mean HFA predictions for each of the four target locations:

$$MD = \sum_{i=1}^{n} \frac{(x_i - \bar{x}_i)^2}{n}$$

To assess similarity in tuning across the two arms, we computed, for each electrode, the SSE (sum of squared errors) for average HFA predictions to the same target between the contralateral and ipsilateral arms.

$$SSE_e = \sum_{i=1}^{n} (\{contra_i - ipsi_i)\}^2$$

This metric was only calculated for the two central targets, the targets common to both arms (the two eccentric target locations varied depending on the arm used). These values were scaled from 0 to 1 based on the minimum and maximum values of SSE across all electrodes. SSE represents a metric of dissimilarity; To calculate a similarity index (SI), we converted this to a measure of similarity by subtracting the scaled SSE values from 1:

$$SI = 1 - \frac{SSE_e - min(SSE_e)}{\max(SSE_e) - (SSE_e)}$$

Thus, higher SI represents more similar average predictions.

Separating instruction and movement phases. The encoding model was run to predict the full HFA time course. To compare model prediction performance during different phases of the task, the data were epoched into instruction and movement phases, using event markers recorded in the analog channel (i.e., cue onset and movement onset). Epochs of the same task phase were concatenated together, and prediction performance was operationalized as the square of the Pearson correlation between the predicted and actual HFA for each task phase.

Permutation testing. A permutation-based analysis-of-variance (pbANOVA) was used to assess differences in distributions for the different experimental conditions. pbANOVA is preferable for experimental designs that involve orthogonal manipulation of fixed factors in which the measured variable does not conform to the distributional assumptions necessary for traditional parametric ANOVA (Anderson & Braak, 2003). In this analysis, null distributions for the main effect of each factor and interaction are created using 10000 surrogate datasets, in each of which the data of a random subset of participants is permuted. In each iteration, the surrogate data is analyzed using a standard ANOVA and the F value of the relevant effect is registered. The effect in the original data is considered significant only if the F value of a standard ANOVA of this effect is larger than 95% of the values in the null distribution. For main effects, the permutations are conducted such that the raw values of the factor of interest are permuted within the levels of the other factor ('restricted' permuting). For the interaction effect, the permutations are not conducted on the raw data but on a dataset that is generated by subtracting the contribution of the main effects from the raw data (see, Anderson & Braak, 2003). The resulting dataset ('reduced' dataset) includes only the interaction terms and their random errors. On this reduced dataset the permutations are conducted without being limited to levels of specific factors ('unrestricted' permutations).

Calculating distance from dorsal central sulcus. For each patient, 30 discrete (x, y) coordinates were manually demarcated along the central sulcus on individual MRI scans. The 30 points were then interpolated to create a line traversing the central sulcus for each individual. The dorsal aspect of the central sulcus was defined as all points dorsal to the midpoint of the central sulcus. We then calculated the absolute distance between each electrode and the closest point on the dorsal aspect of the central sulcus (our interpolated line).

ACKNOWLEDGMENTS:

We want to thank Anwar Nunez-Elizalde for his invaluable guidance building the encoding model, Ian Greenhouse for building the first prototype rig to bring into the ICU and William Liberti for his advice with the figures. This research was supported by the National Institute of Health: NS097480.

AUTHOR CONTRIBUTIONS:

Conceptualization, C.M.M., T.C.D., A.B., J.M.C., R.T.K. and R.B.I.; Methodology, C.M.M., J.M.C., R.B.I; Software, C.M.M.; Investigation, C.M.M.; Resources, J.J.L., E.F.C., D.K-S., K.D.L., and P.B.W.; Writing – Original Draft, C.M.M.; Writing – Review & Editing, T.C.D., A.B., R.T.K., and R.B.I.; Visualization, C.M.M.; Supervision, J.M.C., R.T.K., and R.B.I.; Funding Acquisition, J.M.C., R.T.K., and R.B.I.

DECLARATION OF INTEREST: The authors declare no competing interests.

References:

Nyberg-Hansen, R., & Rinvik, E. (1963). Some comments on the pyramidal tract, with special reference to its individual variations in man. *Acta Neurologica Scandinavica*, *39*(1), 1-30.

Bourbonnais, D., & Noven, S. V. (1989). Weakness in patients with hemiparesis. *American Journal of Occupational Therapy*, *43*(5), 313-319.

Babiloni, C., Carducci, F., Cincotti, F., Rossini, P. M., Neuper, C., Pfurtscheller, G., & Babiloni, F. (1999). Human movement-related potentials vs desynchronization of EEG alpha rhythm: a high-resolution EEG study. *Neuroimage*, *10*(6), 658-665.

Ghacibeh, G. A., Mirpuri, R., Drago, V., Jeong, Y., Heilman, K. M., & Triggs, W. J. (2007). Ipsilateral motor activation during unimanual and bimanual motor tasks. *Clinical Neurophysiology*, *118*(2), 325-332.

Ganguly, K., Secundo, L., Ranade, G., Orsborn, A., Chang, E. F., Dimitrov, D. F., ... & Carmena, J. M. (2009). Cortical representation of ipsilateral arm movements in monkey and man. *Journal of Neuroscience*, *29*(41), 12948-12956.

Ames, K. C., & Churchland, M. M. (2019). Motor cortex signals for each arm are mixed across hemispheres and neurons yet partitioned within the population response. *Elife*, *8*, e46159.

Bundy, D. T., Szrama, N., Pahwa, M., & Leuthardt, E. C. (2018). Unilateral, 3D arm movement kinematics are encoded in ipsilateral human cortex. *Journal of Neuroscience*, *38*(47), 10042-10056.

Wisneski, K. J., Anderson, N., Schalk, G., Smyth, M., Moran, D., & Leuthardt, E. C. (2008). Unique cortical physiology associated with ipsilateral hand movements and neuroprosthetic implications. *Stroke*, *39*(12), 3351-3359.

Cisek, P., Crammond, D. J., & Kalaska, J. F. (2003). Neural activity in primary motor and dorsal premotor cortex in reaching tasks with the contralateral versus ipsilateral arm. *Journal of Neurophysiology*, *89*(2), 922-942.

Steinberg, O., Donchin, O., Gribova, A., De Oliveira, S. C., Bergman, H., & Vaadia, E. (2002). Neuronal populations in primary motor cortex encode bimanual arm movements. *European Journal of Neuroscience*, *15*(8), 1371-1380.

Willett, F. R., Deo, D. R., Avansino, D. T., Rezaii, P., Hochberg, L. R., Henderson, J. M., & Shenoy, K. V. (2020). Hand knob area of premotor cortex represents the whole body in a compositional way. *Cell*, *181*(2), 396-409.

Heming, E. A., Cross, K. P., Takei, T., Cook, D. J., & Scott, S. H. (2019). Independent representations of ipsilateral and contralateral limbs in primary motor cortex. *ELife*, *8*, e48190.

Downey, J. E., Quick, K. M., Schwed, N., Weiss, J. M., Wittenberg, G. F., Boninger, M. L., & Collinger, J. L. (2020). The motor cortex has independent representations for ipsilateral and contralateral arm movements but correlated representations for grasping. *Cerebral Cortex*, *30*(10), 5400-5409.

Corballis, M. C., Badzakova-Trajkov, G., & Häberling, I. S. (2012). Right hand, left brain: genetic and evolutionary bases of cerebral asymmetries for language and manual action. *Wiley Interdisciplinary Reviews: Cognitive Science*, *3*(1), 1-17.

Rothi, L. G., Ochipa, C., & Heilman, K. M. (1997). A cognitive neuropsychological model of limb praxis and apraxia. *Apraxia: The neuropsychology of action*, 29-49.

Schaefer, S. Y., Haaland, K. Y., & Sainburg, R. L. (2007). Ipsilesional motor deficits following stroke reflect hemispheric specializations for movement control. *Brain*, *130*(8), 2146-2158.

Liepmann, H. (1908). *Drei aufsätze aus dem apraxiegebiet* (Vol. 2545). S. Karger.

De Renzi, E., & Lucchelli, F. (1988). Ideational apraxia. *Brain*, *111*(5), 1173-1185.

Haaland, K. Y., Harrington, D. L., & Knight, R. T. (2000). Neural representations of skilled movement. *Brain*, *123*(11), 2306-2313.

Chettouf, S., Rueda-Delgado, L. M., de Vries, R., Ritter, P., & Daffertshofer, A. (2020). Are unimanual movements bilateral? *Neuroscience & Biobehavioral Reviews*, *113*, 39-50.

Verstynen, T., Diedrichsen, J., Albert, N., Aparicio, P., & Ivry, R. B. (2005). Ipsilateral motor cortex activity during unimanual hand movements relates to task complexity. *Journal of Neurophysiology*, *93*(3), 1209-1222.

Verstynen, T., & Ivry, R. B. (2011). Network dynamics mediating ipsilateral motor cortex activity during unimanual actions. *Journal of Cognitive Neuroscience*, *23*(9), 2468-2480.

Schäfer, K., Blankenburg, F., Kupers, R., Grüner, J. M., Law, I., Lauritzen, M., & Larsson, H. B. (2012). Negative BOLD signal changes in ipsilateral primary somatosensory cortex are associated with perfusion decreases and behavioral evidence for functional inhibition. *Neuroimage*, *59*(4), 3119-3127.

Leszczyński, M., Barczak, A., Kajikawa, Y., Ulbert, I., Falchier, A. Y., Tal, I., ... & Schroeder, C. E. (2020). Dissociation of broadband high-frequency activity and neuronal firing in the neocortex. *Science Advances*, *6*(33), eabb0977.

Muthukumaraswamy, S. D. (2010). Functional properties of human primary motor cortex gamma oscillations. *Journal of Neurophysiology*, *104*(5), 2873-2885.

Kriegeskorte, N., & Douglas, P. K. (2019). Interpreting encoding and decoding models. *Current Opinion in Neurobiology*, *55*, 167-179.

Weichert, F., Bachmann, D., Rudak, B., & Fisseler, D. (2013). Analysis of the accuracy and robustness of the leap motion controller. *Sensors*, *13*(5), 6380-6393.

Suway, S. B., & Schwartz, A. B. (2019). Activity in Primary Motor Cortex Related to Visual Feedback. *Cell Reports*, *29*(12), 3872-3884.

Stolk, A., Griffin, S., Van der Meij, R., Dewar, C., Saez, I., Lin, J. J., ... & Oostenveld, R. (2018). Integrated analysis of anatomical and electrophysiological human intracranial data. *Nature Protocols*, *13*(7), 1699-1723.

Canolty, R. T., Edwards, E., Dalal, S. S., Soltani, M., Nagarajan, S. S., Kirsch, H. E., ... & Knight, R. T. (2006). High gamma power is phase-locked to theta oscillations in human neocortex. *Science*, *313*(5793), 1626-1628.

Pei, X., Leuthardt, E. C., Gaona, C. M., Brunner, P., Wolpaw, J. R., & Schalk, G. (2011). Spatiotemporal dynamics of electrocorticographic high gamma activity during overt and covert word repetition. *Neuroimage*, *54*(4), 2960-2972

Hoerl, A. E., & Kennard, R. W. (1970). Ridge regression: Biased estimation for nonorthogonal problems. *Technometrics*, *12*(1), 55-67.

Anderson, M., & Braak, C. T. (2003). Permutation tests for multi-factorial analysis of variance. Journal of statistical computation and simulation, 73(2), 85-113.

Churchland, M. M., Cunningham, J. P., Kaufman, M. T., Foster, J. D., Nuyujukian, P., Ryu, S. I., & Shenoy, K. V. (2012). Neural population dynamics during reaching. *Nature*, *487*(7405), 51-56.

Elsayed, G. F., Lara, A. H., Kaufman, M. T., Churchland, M. M., & Cunningham, J. P. (2016). Reorganization between preparatory and movement population responses in motor cortex. *Nature Communications*, *7*(1), 1-15.

Schaffer, J. E., & Sainburg, R. L. (2021). Interlimb Responses to Perturbations of Bilateral Movements are Asymmetric. *Journal of Motor Behavior*, *53*(2), 217-233.

Diedrichsen, J., Wiestler, T., & Krakauer, J. W. (2013). Two distinct ipsilateral cortical representations for individuated finger movements. *Cerebral Cortex*, *23*(6), 1362-1377.

Przybylski, Ł., & Króliczak, G. (2017). Planning functional grasps of simple tools invokes the hand-independent praxis representation network: an fMRI study. *Journal of the International Neuropsychological Society*, *23*(2), 108-120.

Buxbaum, L. J., Kyle, K. M., Tang, K., & Detre, J. A. (2006). Neural substrates of knowledge of hand postures for object grasping and functional object use: Evidence from fMRI. *Brain Research*, *1117*(1), 175-185.

Xu J, Gannon PJ, Emmorey K, Smith JF, Braun A. Symbolic gestures and spoken language are processed by a common neural system. Proc Natl Acad Sci U S A 2009, 106:20665–20669.

Bohlhalter, S., Hattori, N., Wheaton, L., Fridman, E., Shamim, E. A., Garraux, G., & Hallett, M. (2009). Gesture subtype–dependent left lateralization of praxis planning: An event-related fMRI study. *Cerebral Cortex*, *19*(6), 1256-1262.

Ochipa C, Rothi LJG, Heilman KM (1989): Ideational apraxia—A deficit in tool selection and use. Ann Neurol 25:190–193.

Vingerhoets, G., Acke, F., Alderweireldt, A. S., Nys, J., Vandemaele, P., & Achten, E. (2012). Cerebral lateralization of praxis in right-and left-handedness: Same pattern, different strength. *Human Brain Mapping*, *33*(4), 763-777.

Vingerhoets, G., Alderweireldt, A. S., Vandemaele, P., Cai, Q., Van der Haegen, L., Brysbaert, M., & Achten, E. (2013). Praxis and language are linked: evidence from co-lateralization in individuals with atypical language dominance. *Cortex*, *49*(1), 172-183.

Vingerhoets, G., Acke, F., Alderweireldt, A. S., Nys, J., Vandemaele, P., & Achten, E. (2012). Cerebral lateralization of praxis in right-and left-handedness: Same pattern, different strength. *Human Brain Mapping*, *33*(4), 763-777.

Jäncke, L., Peters, M., Himmelbach, M., Nösselt, T., Shah, J., & Steinmetz, H. (2000). fMRI study of bimanual coordination. *Neuropsychologia*, *38*(2), 164-174.

Toyokura, M., Muro, I., Komiya, T., & Obara, M. (1999). Relation of bimanual coordination to activation in the sensorimotor cortex and supplementary motor area: analysis using functional magnetic resonance imaging. *Brain Research Bulletin*, *48*(2), 211-217.

Serrien, D. J., Cassidy, M. J., & Brown, P. (2003). The importance of the dominant hemisphere in the organization of bimanual movements. *Human Brain Mapping*, *18*(4), 296-305.

Maki, Y., Wong, K. F. K., Sugiura, M., Ozaki, T., & Sadato, N. (2008). Asymmetric control mechanisms of bimanual coordination: an application of directed connectivity analysis to kinematic and functional MRI data. *Neuroimage*, *42*(4), 1295-1304.